Supporting Information for:

Biomolecular interactions on densely coated nanoparticles: a single-molecule perspective

Swayandipta Dey[a,b,#,*], *Rodrigo Rivas-Barbosa*[c,#], *Francesco Sciortino*[c], *Emanuela Zaccarelli*[c,d], *Peter Zijlstra*[a,b,*]

a. Eindhoven University of Technology, Department of Applied Physics and Science Education, Postbus 513, 5600 MB, Eindhoven, The Netherlands.

b. Institute for Complex Molecular Systems and Eindhoven Hendrik Casimir Institute, Eindhoven University of Technology, The Netherlands.

c. Dipartmento di Fisica, Universita' di Roma "La Sapienza", Piazzale Moro 5, Roma I-00185, Italy.

d. CNR Institute of Complex Systems, Uos Sapienza, Piazzale Aldo Moro 2, 00185 Roma, Italy.

*Correspondence to: s.dey@tue.nl and p.zijlstra@tue.nl

Contents

Materials and Methods

Oligonucleotide sequences and sample preparation:

All the oligonucleotide sequences used for the study were commercially purchased from IDT Inc. (Coralville IA, USA). Citrate-stabilized monocrystalline gold nanorods (AC12-40-650, 80nm x 40nm, OD=100) were purchased from Nanopartz. The concentration of gold nanorods (AuNPs) in the working solution was adjusted to OD~1.0 in a buffer mixture of (¼ v/v PBS + ¾ v/v milliQ water) such that it yields a surface coverage of 100 – 200 particles in the 100 x 100 μm^2 field-of-view (FOV) of the microscope after spin-coating. A 50 µL drop of the diluted AuNP suspension was then drop-casted on a coverslip (Menzel, 22 x 22, #1.5) and incubated inside a humidity chamber for 1 hour. For preparing the sample chamber, we used commercially available Secure-Seal Imaging Spacers (SS8X9, Grace Bio-Labs) and Silicone Isolators (Press-To-Seal Silicone Isolator-JTR8R-A-2.5, Grace Bio-Labs).

To ensure that the AuNPs are firmly attached to the substrate, the coverslips were first functionalized with a silanizing agent, (3-Mercaptopropyl) trimethoxysilane, (MPTMS). For the thiolation of the gold nanorods with the silanizing agent (MPTMS), we used the following protocol:

1. Clean coverslips by sonication in Methanol and Isopropyl alcohol, each for 15 mins.

2. Plasma treat the coverslips for 1 min/coverslip.

3. Immerse coverslips in 5% v/v solution of MPTMS in absolute Ethanol for 3 minutes.

4. Rinse coverslips with absolute Ethanol, then air-dry by blowing N_2 to proceed with the functionalization of nanoparticles with ssDNA.

The bio-functionalization of nanoparticles with oligonucleotides was performed using a low-pH protocol. We used a Citric acid buffer of 10 mM strength (pH 3.0, ionic strength 1M), these conditions give very efficient functionalization performance. The total ssDNA concentration was kept constant at 5 µM, even in the case of the mixture of receptor and spacer sequences, where the percentage of receptor sequences was specifically tuned. All the oligo sequences used for this study are shown in **Table S1**. The ssDNA binds to the surface of AuNP via thiol – Au covalent bond. Therefore prior to the functionalization, the thiolated-DNA was incubated in 10 mM of TCEP for 15 minutes to cleave any possible di-thiol bridges. The gold nanoparticles were incubated with thiolated ssDNA for about 3 hours inside a humidity chamber to prevent the sample from possible drying. Immediately after this incubation step, the samples were extensively rinsed with PBS and milliQ to get rid of any residual ssDNA. We performed all our single-particle qPAINT measurements with an imager concentration of 200pM prepared in Buffer B (5mM Tris-HCl, 10mM $MgCl_2.6H_20$, 1mM $Na_2(EDTA).2H_20$; pH = 8.0).

Table S1: DNA sequences used in our experiment

Strand name	Sequence	Modifier
Receptor	**CAT CAT C**AT ACG CTT CCA ATA ATA CAT CTA	5'-thiol
Probe	TAT GTA GAT C	3'-Atto655
10nt Spacer	**CAT CAT C**TA A	5'-thiol
30nt Spacer	**CAT CAT C**TT ACG CTT CCA ATC CCC TCC TCC	5'-thiol
Dye-labeled Receptor	**CAT CAT C**AT ACG CTT CCA ATA ATA CAT CTA	5'-thiol 3'-Atto532

Single molecule Microscopy

The method is based on a single-molecule localization based microscopy (SMLM) technique DNA-PAINT (Point Accumulation In Nanoscale Topography), which was originally developed to count the number of docking strands (receptors) on DNA origami structures.[1,2] For the single particle measurements, we use a quantitative PAINT (qPAINT) fluorescence based microscopy. We apply this method for quantitative analyses of kinetic parameters, i.e. association (k_{on}) and dissociation (k_{off}) rate constants as extracted from our single-particle DNA hybridization experiments.

The AuNPs are functionalized with 30nt receptor sequences, which are mixed with either short 10nt or long 30nt spacers in various dilution ratios such that the resultant (% receptor fractions in the solution = 100, 50, 16, 9, 3). The sample chamber is then mounted onto a stage of an inverted wide-field optical microscope (Nikon-Ti) equipped with an oil-immersive objective (Nikon Apo TIRF 60× Oil, 1.49 NA). We excited the samples with a 637nm CW laser light illumination (Coherent OBIS™ FP 1193837 | 637nm LX 100mW) through an oil-immersion TIRF objective, collected the emitted light with the same objective, and send the wide-field image to a camera (Prime BSI Express Scientific CMOS, Teledyne Photometrics) through a series of dichroic mirror (ZT640rdc-UF2, Chroma Technology), notch (ZET635) and long-pass (FLP635, ThorLabs) filter combination. The perfect focus system (PFS) system was kept on during the acquisition. The fluorescence signal bursts resulted from the transient hybridization between the dye-labeled complementary probes with the receptor sequences immobilized on the surface of AuNPs. An integration time of 100ms was typically used for the detection of single-molecule fluorescence signals. A typical field of view under laser illumination is shown in **Fig.1a** where individual diffraction limited spots correspond to either single particles or clusters.

Single particle intensity-time trajectories (DNA-PAINT)

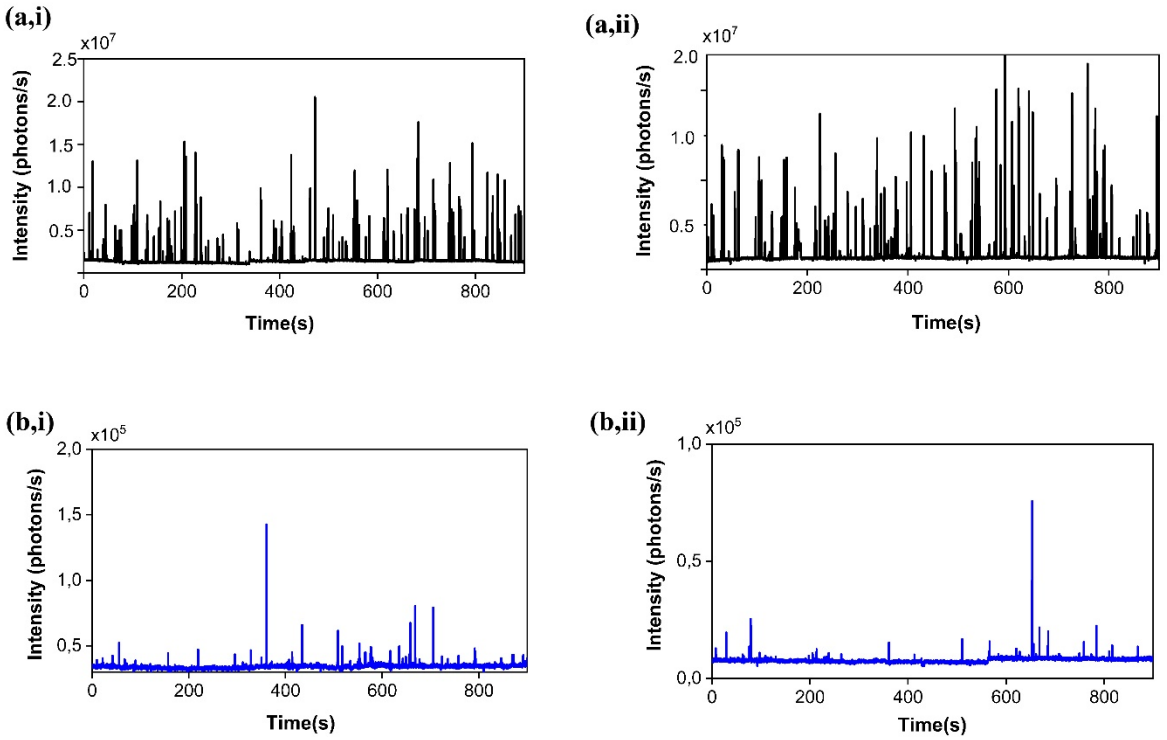

Figure S1 Representative intensity-time trajectories on a single particle from (a) specific binding events and (b) non-specific binding events (performed with a non-complementary imager). Imager concentrations were kept identical at 200pM for these experiments.

Cumulative Distribution Function (CDF) fits of bright times (τ_{bright}, s)

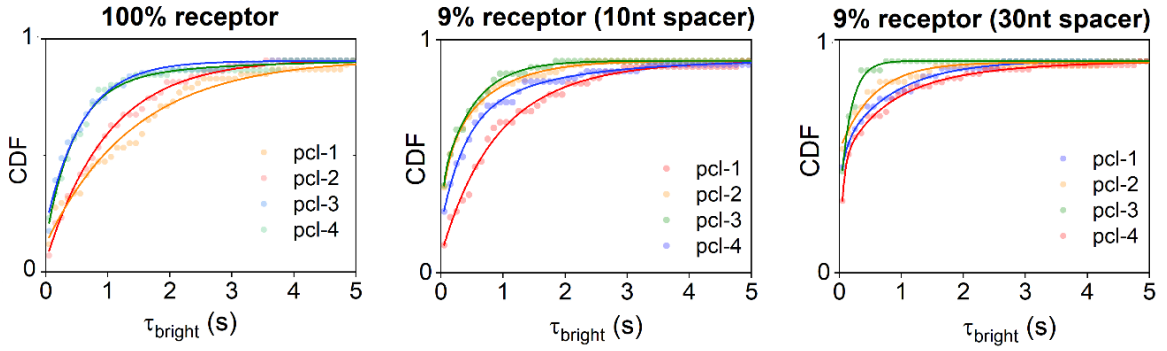

Figure S2 Representative cumulative distribution functions (CDFs) of bright-times and respective fits (shown in bold lines) for few individual particles under different sample conditions as obtained from qPAINT measurements

Distribution of particle surface area and expected rate constants

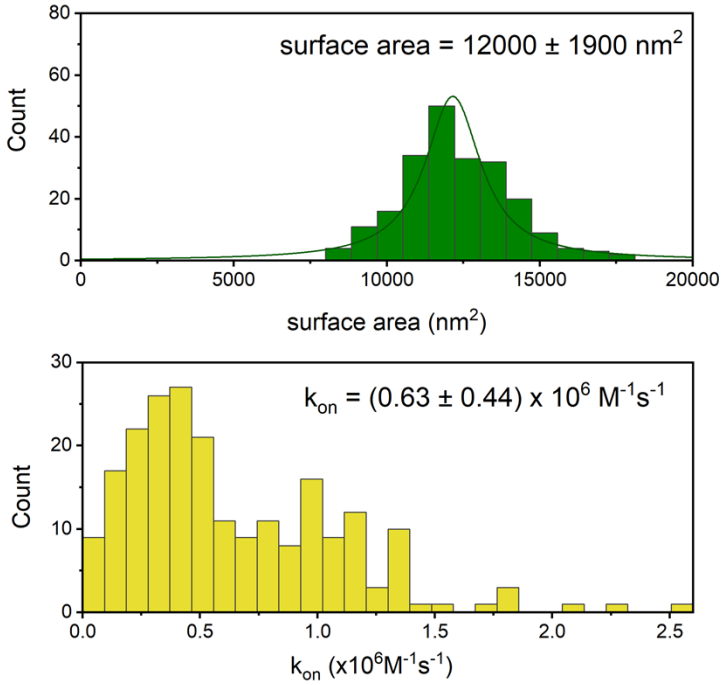

Figure S3 (top panel): Histogram of Au NRs surface area (nm^2) extracted from particle size distribution analysis (SEM measurements), (bottom panel): Histogram of extracted k_{on} values representing the inter-particle variability in the association kinetics

Effect of Electrostatics

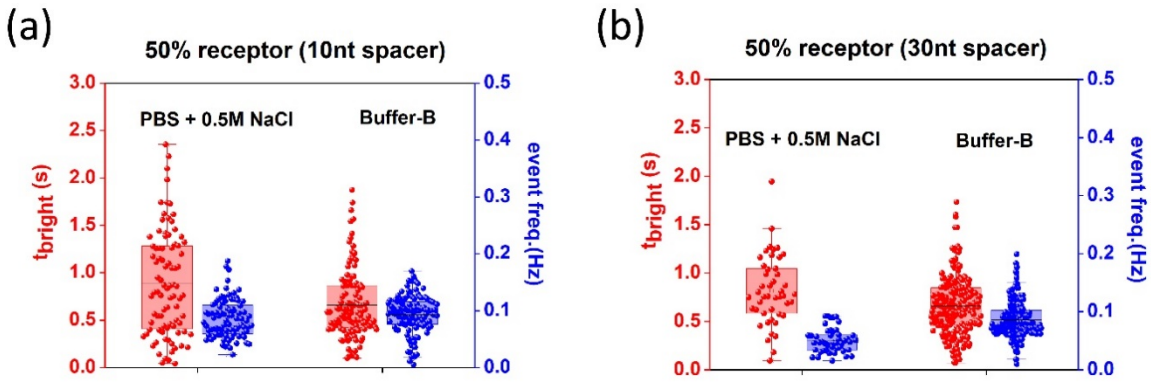

Figure S4. Beeswarm plots showing distribution of bright-times (t_{on}, s) and event frequencies (Hz) under different buffer conditions (PBS+0.5M NaCl and Buffer-B) for (a) 50% receptor (with 10nt spacer) and (b) 50% receptor (with 30nt spacer)

Simulation Methods

Molecular dynamics (MD) simulations of DNA systems were performed using the oxDNA2 model already embedded in the oxDNA simulation package.[3–5] The model describes DNA strands at a nucleotide coarse-grained level. In short, the interactions between nucleotides include stacking, excluded volume, electrostatics and of course sequence dependent hydrogen bonding. All simulations were run on GPUs.

The simulation box had periodic boundary conditions in the "x" and "y" directions; instead, in "z", strands were contained within two repulsive planes both in the upper and lower sides. The box side was 31.5 nm, ensuring no strands interacting with their mirror self and yielding a convenient 100 nm² lid. The simulated area accounts for just a small region of the gold nanorods.

Each system contained N_{probe} =100 probes giving a c_{probe} ~ 5.3 mM concentration; this very high probe concentration enabled gathering binding events faster. The probes, receptors and spacers sequences used are the same as in the experimental setup.

Receptors were fixed to the lower surface via a harmonic potential to an additional "inert" nucleotide in the 5' end playing the role of the thiol; the "inert" nucleotides base wasn't allowed to pair with any other base. Receptors were placed in a square grid. For systems with spacers, receptors were appropriately converted to spacers to reach the desired dilutions.

We used an Anderson-like thermostat with a dt=0.0005 simulation units timestep, roughly 1.51×10^{-15} s.

We used a temperature T=50 °C and salt concentration [NA+] = 0.5 M. Short trial runs at temperatures below 50° C showed very few binding events in our short accessible time window; hence, we decided not to use the experimental temperature to increase the number of events.

We saved the simulation configuration every 5×10^6 steps, corresponding to roughly every 7.6×10^9 s. From the saved configurations we tracked probe-receptor transient binding events in the following way: first, (i) for a single probe and receptor pair, we tracked the complementary sited number of bases paired in time (two bases are said to be paired if the hydrogen bond energy is at least 10% of the fully formed hydrogen bond[6]; then, (ii) consecutive saved frames with at least one base paired were grouped, these being candidate binding events; finally, (iii) all candidate binding events that did not contain a frame with at least 4 bases paired were discarded, these (shorter) rejected events normally corresponding to mismatched probe-receptor hybridization: the receptors base at the 3' end did not pair with the probes 5' end. In the "Height-Based Definition of Binding Events" section we propose an additional transient binding event definition based on the distance of the imager to the surface, somehow closer to the experimental way of detection, nonetheless yielding similar results to the "energy"-based definition used in the main text.

From the tracked binding events we extracted the average bright time, time between consecutive events and event frequency for the simulated systems. The k_{off} was calculated from fitting the histogram of the duration of the binding events to an exponential distribution with mean bright time as the rate parameter

$$f(t;\bar{\tau}) = \bar{\tau}\exp(t/\bar{\tau})$$

Instead, for every start of a binding event, k_{on} was calculated in the following way:

$$k_{on} = (c_{probe}(n_b)\bullet(N_r - n_b)\bullet\Delta t)^{-1}$$

with n_b the number of already existing probe-receptor bonds, $c_{probe}(n_b)$ the unhybridized probe concentration, N_r the total number of receptors, and Δt the time in between the start of two consecutive binding events. The reported k_{on} is the average over all binding events.

Receptor-Spacer Diluted Patterns

When converting receptors into spacers at different dilutions, we decided to choose patterns that maximize the space in between the receptors so that we would decrease competitive effects among them when pairing with the probes. The patterns used are shown in figure S4. The 50% receptor fraction pattern resembles a chessboard; the 10% receptor fraction pattern ensures at least two spacers in between receptors.

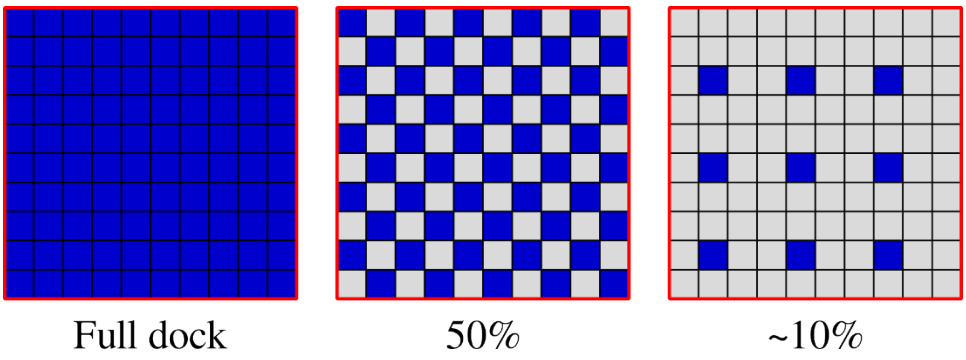

Figure S5. Receptors and spacers pattern for the three different dilutions/receptors fractions. The blue squares indicate receptors and the gray squares spacers.

Height-Based Definition of Binding Events

We propose a second definition of a binding event based on the distance of the probes to the bottom surface. We consider to have a candidate "height" binding event if the "z" component of the center of mass of a probe is below a soft threshold value. We request at least 30 consecutive frames (2.2725×10^{-7} s) below a "soft" threshold value, to say we have a "height"-based binding event candidate. Similarly to the "energy" definition, we impose an additional test to candidate events; in this case we discard all candidate events without a single frame with the imager's z-component below a "hard" threshold value. We choose the threshold values aided from the probes center of mass "z" component density profile (Figure S5). A peak can be seen in the density profile indicating the densest "z"-slice, we assign this distance as the "hard" threshold value. After the peak the profile reaches a plateau, denoting ideal gas-like behavior and the limit of the receptors influence on the probes; this distance is the "soft" threshold value. Figure S6 plots an imagers center of mass "z"-coordinate and number of bases paired as function of time. The "height"-based detected events are marked in red, the "energy"-based events in blue. Both binding definitions detect events in the same time slots and the events are of similar duration. Figure S7 shows the bonded/paired time histogram for both binding definitions, no significant differences can be seen between them. The similarity of results suggests that events detected experimentally happens not only due to the probes proximity to the nanorods, but also due to an actual hybridization.

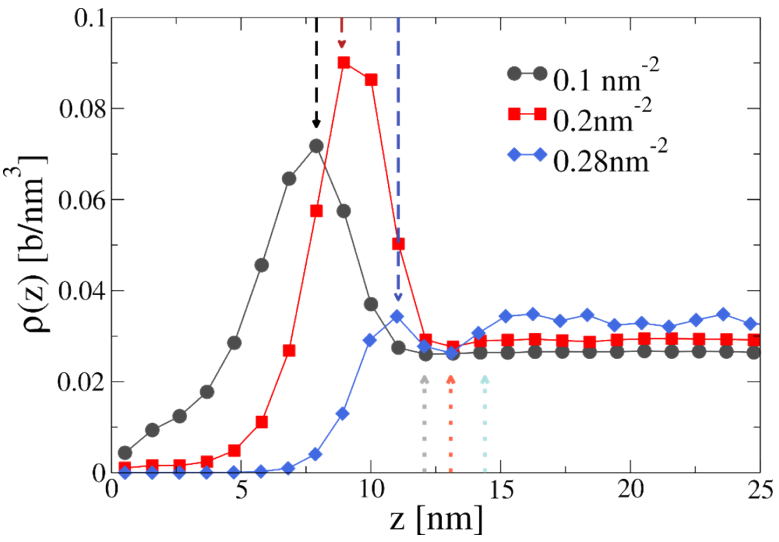

Figure S6. Probes "z" density profile for 100% receptors coating at different surface densities. The similarly colored arrows coming from the top (bottom) indicate the hard (soft) threshold value picked.

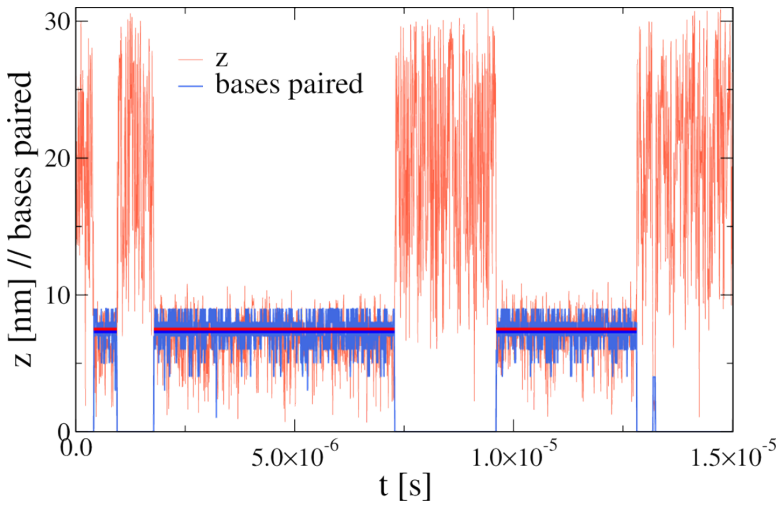

Figure S7. Tracking of the imagers z-coordinate (light red) and number of bases (light blue) in time. The detected events by the "height" ("energy") definition are marked with a darker red (blue) horizontal line.

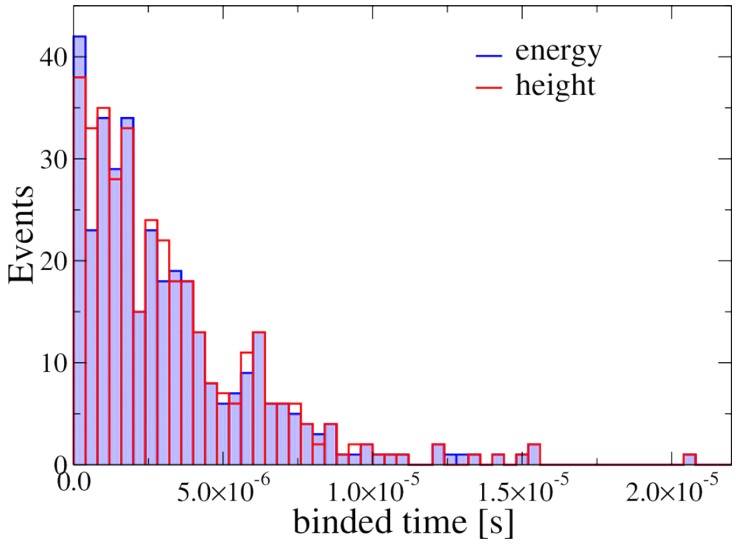

Figure S8. Bonded time distribution according to the energy- and height-based definitions (blue and red respectively) for a 0.1 nm^{-2} surface density system coated 100% with receptors.

Surface Strands Height of the Last 9 Bases

Figure S5 shows the center of mass z-coordinate distribution of the last 9 bases of the surface strands (receptors and 30nt spacers) for the different dilutions. On average, the position of these last 9 bases does not change between

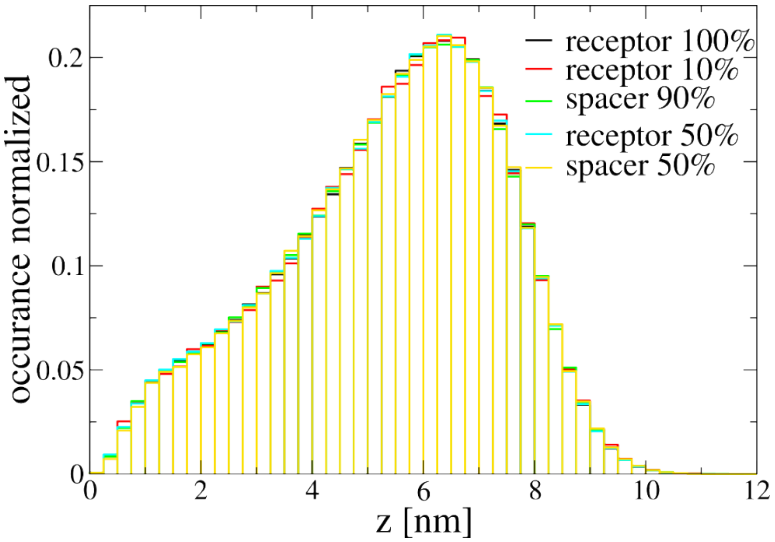

species or dilution.

Figure S9. Height distribution from the surface of the last 9 nucleotides (3'). Simulations with no probes.

Base pairing maps

Figure S9 shows the energy-weighted base pairing maps between receptor-receptor, receptor-spacer and spacer-spacer for a 0.1 nm^{-2} surface density at the three spacer dilutions in the absence of probes. The occurrence of the base pairing is weighted with the average energy of the bond. The largest pairing contributions come from bases 18 with 17 and 19 in (5' to 3'), which corresponds to a C-G base pairing. Being consecutive bases, the pairing cannot be of a single receptor with itself but must be with another receptor; these receptor-receptor pairing decrease with dilution due to the increasing distance between them (the layout of the receptor/spacer plays an important role); nonetheless, for the diluted systems, the mix species receptor-spacer base pairing of these bases compensate. Interactions between receptors and spacers are in general different, but the maps do not give evidence that surface strand base pairing leads to an increase in k_{on} with dilution.

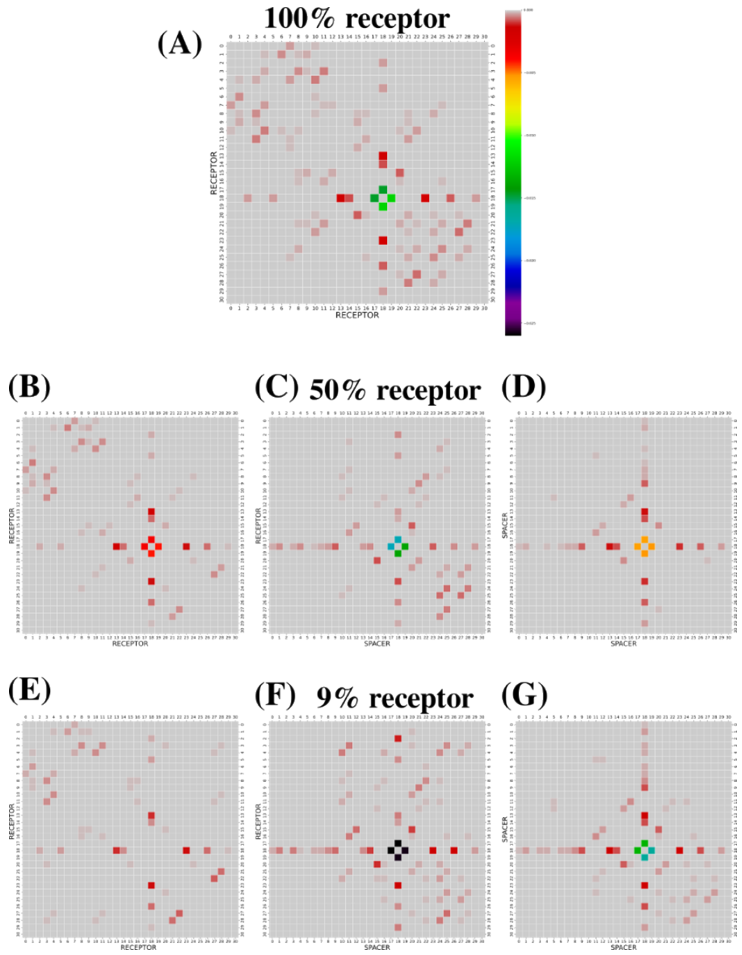

Figure S10. Base pairing maps for the different dilutions and receptor-receptor, receptor-spacer and spacer-spacer interactions. (A) Receptor-receptor map for a 100% receptor surface. (B) Receptor-receptor, (C) receptor-spacer, and (D) spacer-spacer for a 50% receptor surface. (E) Receptor-receptor, (F) receptor-spacer, and (G) spacer-spacer for a 9% receptor surface. Bases are labeled from 0 to 30 in the 3' - 5' direction.

Dissociation Rate as Function of the Bases Paired

Exploring the possible reasons behind the increase in k_{off} for the 0.28 nm^{-2} system, we investigated the base paring during binding events. Figure S10 shows the average number of bases paired during an event at the different dilutions and surface densities including the limiting case of a single receptor (~0.001 nm^{-2}). The number of bases paired is the same (~7.3) for all but the densest coating density, with a smaller ~7.15, consistent with the higher k_{off}.

Figure S11 shows the occurrence fraction of the complementary sites during binding events for the different coating densities. We can see that the last 6 bases away from the surface have a similar occurrence at all densities, but as we move closer to the nanorod surface, deviations begin only for the densest 0.28 nm^{-2} system. In fact, the differences increase the closer to the surface, base pairing becomes harder for the closer to the surface bases. The average smaller number of bases paired for the densest surface translates in the increase of k_{off}. It is interesting to notice that unlike k_{on}, the crowding effects on k_{off} are only perceptible for this very dense system.

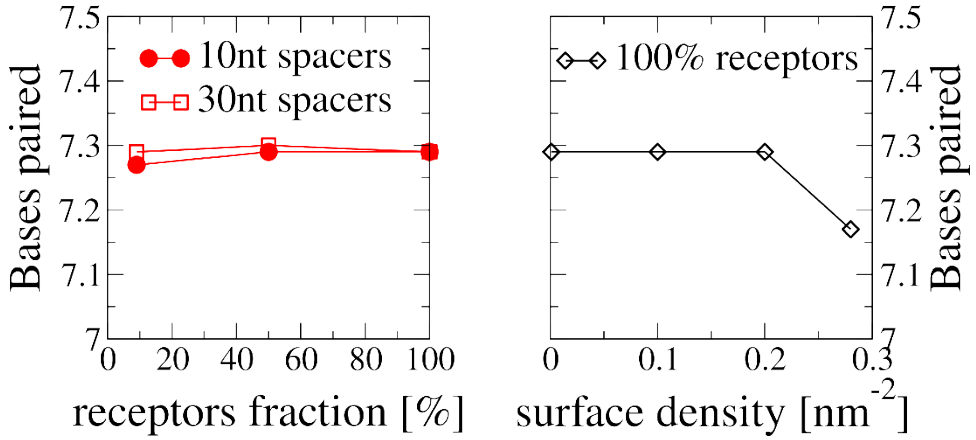

Figure S11. Bases paired as function of **(A)** fraction of docks for a 0.1 nm^{-2} surface density diluted with spacers (red symbols) and **(B)** surface density (black symbols), the first point corresponds to a single receptor ~0.001 nm^{-2} .

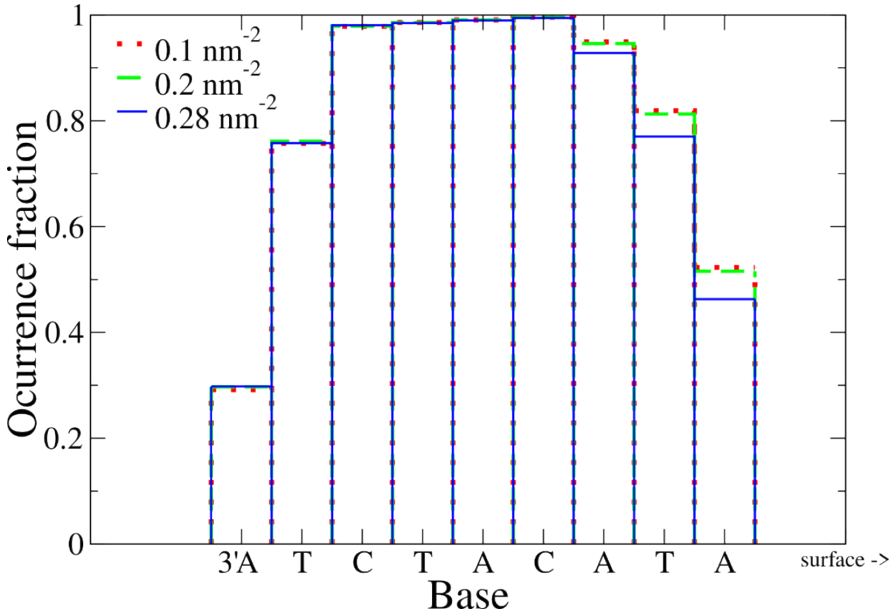

Figure S12. Receptor base pairing occurrence fraction during binding events for the different surface densities.

Simple Binding Model

Theory

Let us consider a simple toy model: a system of volume V composed of a single fixed binding site and free particles. The free particles behave like an ideal gas in all ways except that they can get trapped inside the binding site of binding volume V_b and binding energy $-\epsilon$. We can think of the free-roaming particles and the fixed binding site, respectively, as the *imagers* and a *dock* in the experimental set-up. To mimic the pairing behavior of dsDNA, we impose the single-bond per particle condition, i.e. the binding site can at most be occupied by one particle. Due to the binding site single-bond condition, the system can be in only one of two states, either *bonded* or *open*. The grand canonical partition function is then given by only two terms:

$$X_i(V,T,\mu) = \sum_{N=0}^{\infty} \frac{z^N}{N!} Z_N = z^0 Z_0 + z Z_1$$
$$= 1 + z V_b e^{\beta \in}$$
$$= 1 + \rho V_b e^{\beta \in} \qquad (1)$$

where z is the activity, which for an ideal gas is equal to the number density $z = \rho = N_i/V$.
The probability of finding the system in the *bonded* state, i.e. with the binding site occupied, is then given by

$$p_b = \frac{\frac{N_i}{V} V_b e^{\beta \in}}{1 + \frac{N_i}{V} V_b e^{\beta \in}} = \frac{V_b e^{\beta \in}}{\frac{V}{N_i} + V_b e^{\beta \in}} . \qquad (2)$$

Similarly, the bonded state probability can be written as function of the average bright (bonded) and dark (unbonded) times, $\langle t_b \rangle$ and $\langle t_d \rangle$ respectively, like

$$p_b = \frac{\langle t_b \rangle}{\langle t_b \rangle + \langle t_d \rangle} \qquad (3)$$

Comparing both equations, other than from a constant κ, we can identify the terms as:

$$\langle t_b \rangle = \frac{1}{\kappa} V_b e^{\beta \varepsilon} \tag{4}$$

and

$$\langle t_d \rangle = \frac{1}{\kappa} \frac{V}{N_i} = \frac{1}{\kappa' . C_i} . \tag{5}$$

The average bright time $\langle t_b \rangle$ depends on the binding volume and temperature, while the average dark time $\langle t_d \rangle$ is inversely proportional to the number density.

Now, let us consider that the system is not composed of a single binding site, but by N_d of them. Assuming like in the experimental set-up that no simultaneous binding events take place, then the average surface open time $\langle t_d \rangle_{Nd}$ is just the single site average time divided by the total number of sites in the surface:

$$\langle t_d \rangle_{N_d} = \frac{\langle t_d \rangle}{N_d} = \frac{V}{\kappa N_i N_d} = \frac{1}{\kappa' C_i N_d} . \tag{6}$$

After identifying the model's constant κ with the association rate k_{on} we reach the same expression for the surface open (*off*) time

$$\tau_{off} = \frac{1}{k_{on} C_i N_d} .$$

Temperature Difference

The experimental measurements were performed at ~ 20°C, while oxDNA2 simulations were at 50°C in order to increase the number of events but shorten their duration. Additionally, the probes numerical concentration was about 5 mM instead of 0.2 nM. The five orders in magnitude difference between in the k_{off} can then be ascribed to these differences in the setups as shown in figure S12 below:

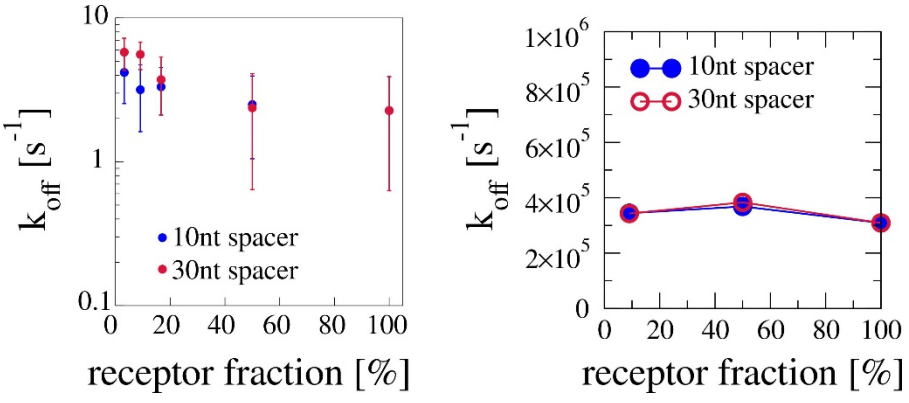

Given that the dissociation rate is the inverse of the average bright time (eq. 4) and the binding energy to the enthalpic contribution to the change of free energy between the bound and unbound states $\in = \Delta H =$ -57.4, as calculated from SantaLucia nearest neighbours model[7,8], the estimated ratio of the dissociation rate k_{off} using the experimental and numerical temperatures (T = 20^0C and 50^0C, respectively) is

$$\frac{k_{off}(T_{20})}{k_{off}(T_{50})} = exp\left[\frac{-\Delta H}{k_B}\left(\frac{1}{323} - \frac{1}{293}\right)\right] \approx 1.0\ x\ 10^{-4} \quad (7)$$

Figure S13. Comparison between the experimental and numerical dissociation rates as a function of receptor fraction.

which is still an order of magnitude smaller than what found in the experiments. However, it is likely possible that the remaining difference comes from the higher concentration used in the simulations.

References

1 R. Jungmann, C. Steinhauer, M. Scheible, A. Kuzyk, P. Tinnefeld and F. C. Simmel, *Nano Lett.*, 2010, **10**, 4756–4761.

2 R. Jungmann, M. S. Avendaño, M. Dai, J. B. Woehrstein, S. S. Agasti, Z. Feiger, A. Rodal and P. Yin, *Nature Methods*, 2016, **13**, 439–442.

3 T. E. Ouldridge, A. A. Louis and J. P. K. Doye, *The Journal of Chemical Physics*, 2011, **134**, 085101.

4 A. Sengar, T. E. Ouldridge, O. Henrich, L. Rovigatti and P. Šulc, *Frontiers in Molecular Biosciences*.

5 B. E. K. Snodin, F. Randisi, M. Mosayebi, P. Šulc, J. S. Schreck, F. Romano, T. E. Ouldridge, R. Tsukanov, E. Nir, A. A. Louis and J. P. K. Doye, *The Journal of Chemical Physics*, 2015, **142**, 234901.

6 M. C. Engel, D. M. Smith, M. A. Jobst, M. Sajfutdinow, T. Liedl, F. Romano, L. Rovigatti, A. A. Louis and J. P. K. Doye, *ACS Nano*, 2018, **12**, 6734–6747.

7 J. SantaLucia, *Proceedings of the National Academy of Sciences*, 1998, **95**, 1460–1465.

8 J. SantaLucia and D. Hicks, *Annu. Rev. Biophys. Biomol. Struct.*, 2004, **33**, 415–440.